

# Towards Robust Detection of Adversarial Examples

Tianyu Pang<sup>1</sup> Chao Du<sup>1</sup> Yinpeng Dong<sup>1</sup> Jun Zhu<sup>1</sup>

## Abstract

Although the recent progress is substantial, deep learning methods can be vulnerable to the maliciously generated adversarial examples. In this paper, we present a novel training procedure and a thresholding test strategy, towards robust detection of adversarial examples. In training, we propose to minimize the reverse cross-entropy, which encourages a deep network to learn latent representations that better distinguish adversarial examples from normal ones. In testing, we propose to use a thresholding strategy as the detector to filter out adversarial examples for reliable predictions. Our method is simple to implement using standard algorithms, with little extra training cost compared to the common cross-entropy minimization. We apply our method to defend various attacking methods on the widely used MNIST and CIFAR-10 datasets, and achieve significant improvements on robust predictions under all the threat models in the adversarial setting.

## 1. Introduction

Deep learning (DL) has obtained unprecedented progress in various tasks, including image classification, speech recognition, and natural language processing (Goodfellow et al., 2016). However, a high-accuracy DL model can be vulnerable in the adversarial setting (Szegedy et al., 2014; Goodfellow et al., 2015), where adversarial examples are maliciously generated to mislead the model to output wrong predictions. Several attacking methods have been developed to craft such adversarial examples (Goodfellow et al., 2015; Kurakin et al., 2017a; Liu et al., 2017; Papernot et al., 2016a;b; Carlini & Wagner, 2017a). As DL is becoming ever more prevalent, it is imperative to improve the robustness, especially in critical regions (e.g., self-driving cars, healthcare and finance).

Therefore, various defenses have been proposed attempting to correctly classify adversarial examples (Szegedy et al.,

<sup>1</sup>Dept. of Comp. Sci. & Tech., TNList Lab, State Key Lab for Intell. Tech. & Systems, CBICR Center, Tsinghua University. Correspondence to: Jun Zhu <dcsjz@mail.tsinghua.edu.cn>.

2014; Gu & Rigazio, 2014; Papernot et al., 2016c; Rozsa et al., 2016; Zheng et al., 2016). However, most of these defenses are not effective enough, which can be successfully attacked by more powerful adversaries (Carlini & Wagner, 2017a;b). Overall, as adversarial examples always exist for a fixed parametric model (thus fixed decision boundaries), it is unlikely for such methods to solve the problem by preventing adversaries from generating adversarial examples, no matter how hard it is to find them.

Due to the difficulty, recent work on defense has turned to detecting adversarial examples instead. Grosse et al. (2017) introduce an extra class in classifiers solely for adversarial examples, and similarly Gong et al. (2017) train an additional binary classifier to decide whether the instance is adversarial or not. Metzen et al. (2017) detect adversarial examples via training a detection neural network, which takes input from intermediate layers of the classification network. Bhagoji et al. (2017) reduce dimensionality of the input image fed to the classification network, and train a fully-connected neural network on the smaller input. Li & Li (2016) build a cascade classifier where each classifier is implemented as a linear SVM acting on the PCA of inner convolutional layers of the classification network. The aforementioned methods all require large extra computational cost, while some of them also result in loss of accuracy on normal examples. Feinman et al. (2017) propose a kernel density estimate method to detect the points lying far from the data manifolds in the final-layer hidden space, which does not change the structure of the classification network with little extra computational cost. They also combine with a Bayesian uncertainty estimate method which is only available on dropout neural networks (Li & Gal, 2017). However, Carlini & Wagner (2017b) show that each of these defense methods can be evaded by an adversary targeting at that specific defense. In this paper, we make contributions by presenting a new method that consists of a novel training procedure and a thresholding test strategy. Our method provides a robust way to detect adversarial examples.

In training, we propose to minimize a novel objective function, named as reverse cross-entropy (RCE), instead of minimizing the common cross-entropy (CE) loss (Goodfellow et al., 2016). By minimizing RCE, our training procedure encourages the classifiers to return a high confidence on the true class while a uniform distribution on false classes for

each data point, and further makes the classifiers map the normal examples to the neighborhood of low-dimensional manifolds in the final-layer hidden space. The minimization of RCE is simple to implement using stochastic gradient descent methods, with little extra training cost, as compared to CE. Therefore, it can be easily applied to any deep networks.

In testing, we propose a thresholding strategy as the detector based on the kernel density estimate method, which has shown its superiority and versatility compared to other detection-based defense methods (Feinman et al., 2017; Carlini & Wagner, 2017b). By setting a proper threshold, we can filter out adversarial examples for robust predictions, namely, we make the classifiers return meaningful predictions only when values of kernel density are higher than a given threshold, and otherwise refuse to predict.

We apply our method to defend various attacking methods on the widely used MNIST (LeCun et al., 1998) and CIFAR-10 (Krizhevsky & Hinton, 2009) datasets. We test the performance of our method under different threat models, i.e., *oblivious adversaries*, *white-box adversaries* and *black-box adversaries* (Carlini & Wagner, 2017b). The results show that the proposed method improves the robustness against adversarial attacks under all the threat models, while maintaining state-of-the-art accuracy on normal examples.

## 2. Background

This section provides the background knowledge on the notations, as well as the definition of threat models and different attacking methods used in this paper.

### 2.1. Notations

A deep neural network (DNN) classifier can be generally expressed as a mapping function  $F(X, \theta) : \mathbb{R}^d \rightarrow \mathbb{R}^L$ , where  $X \in \mathbb{R}^d$  is the input variable,  $\theta$  denotes all the parameters and  $L$  is the number of classes (hereafter we will omit  $\theta$  without ambiguity). Here, we focus on the DNNs with softmax output layers. For notation clarity, we define the softmax function  $\mathbb{S}(z) : \mathbb{R}^L \rightarrow \mathbb{R}^L$  as  $\mathbb{S}(z)_i = \exp(z_i) / \sum_{i=1}^L \exp(z_i)$ ,  $i \in [L]$ , where  $[L] := \{1, \dots, L\}$ . Let  $Z$  be the output vector of the penultimate layer, i.e., the final hidden layer. This defines a mapping function:  $X \rightarrow Z$  to extract data representations. Then, the classifier can be expressed as  $F(X) = \mathbb{S}(W_s Z + b_s)$ , where  $W_s$  and  $b_s$  are the weight matrix and bias vector of the softmax layer respectively. We denote the pre-softmax output  $W_s Z + b_s$  as  $Z_{pre}$ , termed logits. Given an input  $x$  (i.e., an instance of  $X$ ), the output of the classifier is a  $L$ -dimensional probability vector, with each element  $F(x)_i$  being the probability that  $x$  belongs to class  $i$ . The predicted label for  $x$  is denoted as  $\hat{y} = \arg \max_i F(x)_i$ . The probability value  $F(x)_{\hat{y}}$  is often used as the corresponding confidence score on this

prediction (Goodfellow et al., 2016).

Let  $Z_{pre,i}, i \in [L]$  be the  $i$ th element of  $Z_{pre}$ , then the decision boundary between each pair of the two classes  $i$  and  $j$  is the hyperplane decided by  $\{z : Z_{pre,i} = Z_{pre,j}\}$ , denoted as  $db_{ij}$ . We let  $DB_{ij} = \{Z_{pre,i} = Z_{pre,j} + C, C \in \mathbb{R}\}$  be the set of all parallel hyperplanes w.r.t.  $db_{ij}$ . Furthermore, we denote the half space  $Z_{pre,i} \geq Z_{pre,j}$  as  $db_{ij}^+$ , where we can formally represent any decision region of class  $\hat{y}$  as  $dd_{\hat{y}} = \bigcap_{i \neq \hat{y}} db_{\hat{y}i}^+$  and the corresponding decision boundary of this region as  $\overline{dd_{\hat{y}}}$ .

Let  $\mathcal{D} := \{(x_i, y_i)\}_{i \in [N]}$  be a training set with  $N$  input-label pairs, where  $y_i \in [L]$  is the true class of  $x_i$ . One common training objective is to minimize the cross-entropy (CE) loss, which is defined as:

$$\mathcal{L}_{CE}(x, y) = -1_y \cdot \log F(x) = -\log F(x)_y,$$

for a single pair  $(x, y)$ , where  $1_y$  is the one-hot encoding of  $y$ . The CE training procedure intends to minimize the average CE loss to obtain the optimal parameters  $\theta^* = \arg \min_{\theta} \frac{1}{N} \sum_{i \in [N]} \mathcal{L}_{CE}(x_i, y_i)$ , which can be efficiently done by stochastic gradient methods with back-propagation (Kingma & Ba, 2015; Rumelhart et al., 1988).

### 2.2. Threat models

In the adversarial setting, a suitable and elaborate taxonomy of threat models is introduced in Carlini & Wagner (2017b):

- **Oblivious adversaries** are not aware of the existence of the detector  $D$  and generate adversarial examples based on the unsecured classification model  $F$ .
- **White-box adversaries** know the scheme and parameters of  $D$ , and can design specific methods to attack both the classification model  $F$  and the detector  $D$  simultaneously.
- **Black-box adversaries** know the existence of the detector  $D$  with its scheme, but have no access to the parameters of the detector  $D$  or the model  $F$ .

### 2.3. Attacking methods

Although DNNs have obtained substantial progress, adversarial examples can be easily identified to fool the network, even when its accuracy is high (Nguyen et al., 2015). Several attacking methods on generating adversarial examples have been introduced in recent years. Most of them can craft adversarial examples that are visually indistinguishable from the corresponding normal ones, and yet are misclassified by the target model  $F$ . Here we introduce some well-known and commonly used attacking methods.

**Fast Gradient Sign Method (FGSM):** Goodfellow et al. (2015) introduce an one-step attacking method. Given a

normal input  $x$  and a classification model with loss  $\mathcal{L}(x, y)$ , the adversarial example is crafted as

$$x^* = x + \epsilon \operatorname{sign}(\nabla_x \mathcal{L}(x, y)),$$

with small perturbation  $\epsilon$ . This method is extremely fast and can fool trained DNNs with a relatively high success rate.

**Basic Iterative Method (BIM):** Kurakin et al. (2017a) propose an iterative version of FGSM, termed Basic Iterative Method. BIM has the recursive formula as

$$x_i^* = \operatorname{clip}_{x, \epsilon}(x_{i-1}^* + \epsilon \operatorname{sign}(\nabla_{x_{i-1}} \mathcal{L}(x_{i-1}^*, y))),$$

where  $x_0^* = x$  and  $\operatorname{clip}_{x, \epsilon}(\cdot)$  is a clipping function that keeps adversarial examples within the  $\epsilon$ -neighborhood of  $x$ .

**Iterative Least-likely Class Method (ILCM):** Kurakin et al. (2017a) also propose a targeted version of BIM. In this method the recursive formula becomes

$$x_i^* = \operatorname{clip}_{x, \epsilon}(x_{i-1}^* - \epsilon \operatorname{sign}(\nabla_{x_{i-1}} \mathcal{L}(x_{i-1}^*, y_{ll}))),$$

where  $x_0^* = x$  and  $y_{ll} = \arg \min_i F(x)_i$ . ILCM can avoid label leaking (Kurakin et al., 2017b), since it does not use the true label  $y$  when crafting adversarial examples.

**Jacobian-based Saliency Map Attack (JSMA):** Papernot et al. (2016b) propose another iterative method for targeted attack, which perturbs one feature  $x_i$  by a constant offset  $\epsilon$  in each iteration step,  $i \in [d]$ . The feature to perturb in each iteration is the one that maximizes the saliency map

$$S(X, t)[i] = \begin{cases} 0, & \text{if } \frac{\partial F(X)_t}{\partial X_i} < 0 \text{ or } \sum_{j \neq t} \frac{\partial F(X)_j}{\partial X_i} > 0 \\ \left( \frac{\partial F(X)_t}{\partial X_i} \right) \left| \sum_{j \neq t} \frac{\partial F(X)_j}{\partial X_i} \right|, & \text{otherwise} \end{cases}$$

for each input feature  $x_i$ . JSMA perturbs much less pixels compared to other methods.

**Carlini & Wagner (C&W):** Carlini & Wagner (2017a) introduce an optimization-based method, which is one of the most powerful attacks. They define  $x^* = \frac{1}{2}(\tanh(\omega) + 1)$  in terms of an auxiliary variable  $\omega$ , and solve

$$\min_{\omega} \frac{1}{2}(\tanh(\omega) + 1) - x \parallel^2_2 + c \cdot f\left(\frac{1}{2}(\tanh(\omega) + 1)\right),$$

where  $c$  is a constant that need to be chosen by modified binary search.  $f(\cdot)$  is an objective function as

$$f(x) = \max(\max\{Z_{pre}(x)_i : i \neq t\} - Z_{pre}(x)_i, -\kappa),$$

where  $\kappa$  controls the confidence on adversarial examples.

Note that both JSMA and C&W do not rely on the training loss  $\mathcal{L}(x, y)$ , which indicates that these attacks are independent of the training procedures of the target networks.

### 3. Methodology

In this section, we present a new method to improve the robustness of classifiers against adversarial examples. We first provide some insights on the existence of adversarial examples and the insufficiency of confidence score as a thresholding metric, which guide us to the new method.

#### 3.1. The intrinsic existence of adversarial examples

Previous work (Goodfellow et al., 2015; Papernot et al., 2016b) hypothesizes that the existence of adversarial examples is caused by certain defects in the training phase. One main support is from the universal approximator theorem (Hornik et al., 1989) that DNNs are able to represent functions that resist adversarial examples. However, in practice any given DNN has an architecture of limited scale, which results in a limited representation capability, and the existence of adversarial examples is intrinsic, as explained below. For a given DNN classifier, its decision boundaries are fixed. Then, any pair of similar instances located on different sides of a decision boundary will be classified into different classes. Very often, such a pair of input points are not distinguishable by human observers; thus, it sounds counterintuitive and irrational to have a jump on the predicted labels. Previous works that attempt to classify adversarial examples correctly (Szegedy et al., 2014; Gu & Rigazio, 2014; Papernot et al., 2016c) will only result in the change of the distribution of decision boundaries but the jump on the predicted labels nearby the decision boundaries still exists. Therefore, a smart enough adversary can always find new adversarial examples to successfully attack the target classifier no matter how the decision boundaries change, as has been demonstrated in (Szegedy et al., 2014).

#### 3.2. The insufficiency of confidence and a new metric

In consideration of the intrinsic existence of adversarial examples, we design a defense strategy to detect adversarial examples instead, which can help the classifiers distinguish adversarial examples from normal ones so as to filter them out for robust predictions.

Preliminarily, we need some metrics to decide whether an input  $x$  is adversarial or not for a given classifier  $F(X)$ . A potential candidate is the confidence  $F(x)_y$  on the predicted label  $\hat{y}$ , which inherently conveys the degree of certainty on a prediction and has in fact been widely used (Goodfellow et al., 2016). As  $F$  predicts incorrectly on adversarial examples, intuitively we should expect a higher confidence on a normal example than that on an adversarial example, which consequently allows us to distinguish them by the confidence values. However, it has been shown that a well-trained DNN classifier usually not only misclassifies adversarial examples but also gives high confidence on its

predictions (Goodfellow et al., 2015; Nguyen et al., 2015), which renders the confidence unreliable in the adversarial setting. This is because in the normal setting without adversaries, the distribution of the test data is similar with that of the training data, then a high confidence implies a high probability to be a correct prediction. In the adversarial setting, adversaries can explore the points far from the data distribution (Li & Gal, 2017), and the predictions in these regions mostly result from extrapolation with high uncertainty. Therefore, a high confidence returned in these regions is unreliable and probably a false positive.

Since the unreliability of using the confidence as a single metric in the adversarial setting, we construct another metric which is more pertinent and helpful to our goal. Namely, we define the metric of *non-ME*—the entropy of normalized non-maximal elements in  $F(x)$ , as:

$$\text{non-ME}(x) = - \sum_{i \neq \hat{y}} \hat{F}(x)_i \log(\hat{F}(x)_i), \quad (1)$$

where  $\hat{F}(x)_i = F(x)_i / \sum_{j \neq \hat{y}} F(x)_j$  are the normalized non-maximal elements in  $F(x)$ . Hereafter we will consider in the final-layer hidden space of  $F$ , and do not distinguish between the input vector  $x$  and its corresponding final hidden vector  $z$  without ambiguity. Note that the output  $F(z)$  has  $L - 1$  equal non-maximal elements on the low-dimensional manifold  $S_{\hat{y}} = (\bigcap_{i,j \neq \hat{y}} db_{ij}) \cap dd_{\hat{y}}$ , so we have Lemma 1:

**Lemma 1.** (Proof in Appendix) *In the decision region  $dd_{\hat{y}}$  of class  $\hat{y}$ ,  $\forall i, j \neq \hat{y}, db_{ij} \in DB_{ij}$ , the value of non-ME on any low-dimensional manifold  $\bigcap_{i,j \neq \hat{y}} db_{ij}$  is constant. In particular, non-ME obtains its global maximal value  $\log(L - 1)$  on and only on  $S_{\hat{y}}$ .*

When  $S_{\hat{y}}$  is empty, the conclusion of Lemma 1 becomes trivial, thus after this we consider the non-trivial cases where  $S_{\hat{y}} \neq \emptyset$ . Lemma 1 tells us that in the decision region of class  $\hat{y}$  if one moves a normal input along the low-dimensional manifold  $\bigcap_{i,j \neq \hat{y}} db_{ij}$ , then its value of non-ME will not change. This conclusion leads to Theorem 1 as below:

**Theorem 1.** (Proof in Appendix) *In the decision region  $dd_{\hat{y}}$  of class  $\hat{y}$ ,  $\forall i, j \neq \hat{y}, z_0 \in dd_{\hat{y}}$ , there exists a unique  $db_{ij}^0 \in DB_{ij}$ , such that  $z_0 \in Q_0$ , where  $Q_0 = \bigcap_{i,j \neq \hat{y}} db_{ij}^0$ . Let  $Q_0^{\hat{y}} = Q_0 \cap \overline{dd_{\hat{y}}}$ , then the solution set of the problem*

$$\arg \min_{z_0} \left( \max_{z^* \in Q_0^{\hat{y}}} F(z^*)_{\hat{y}} \right)$$

is  $S_{\hat{y}}$ . Furthermore  $\forall z_0 \in S_{\hat{y}}$  there is  $Q_0 = S_{\hat{y}}$ , and  $\forall z^* \in S_{\hat{y}} \cap \overline{dd_{\hat{y}}}, F(z^*)_{\hat{y}} = \frac{1}{L}$ .

Let  $z_0$  be a given normal example with the predicted class  $\hat{y}$ , and  $\max_{z^* \in Q_0^{\hat{y}}} F(z^*)_{\hat{y}}$  represents the maximal value of confidence obtained when moving  $z_0$  along  $Q_0$  to reach the

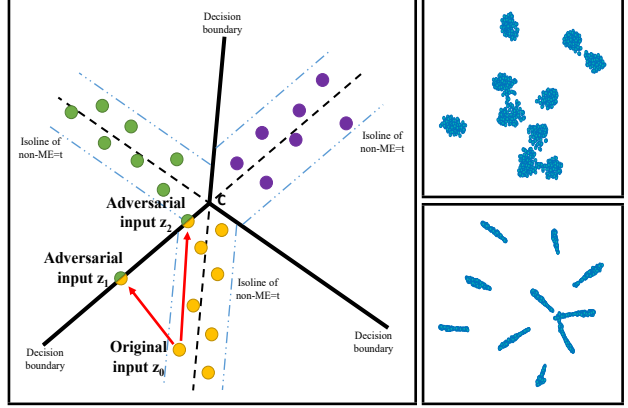


Figure 1. (Left) The black solid lines are the decision boundaries, the black dashed lines are the decision boundaries between two classes. The blue dot-dashed lines are the isolines of non-ME =  $t$ . (Right) t-SNE visualization of the final hidden vectors on CIFAR-10. The model is Resnet-32. The training procedure of the upper panel is CE and of the lower panel is RCE.

decision boundary  $\overline{dd_{\hat{y}}}$ . Theorem 1 tells us that there exists a unique low-dimensional manifold  $Q_0$  that  $z_0$  lies on in the decision region of class  $\hat{y}$ , and if we can somehow restrict adversaries changing the values of non-ME when generating adversarial examples by moving or perturbing  $z_0$ , then on the set  $S_{\hat{y}}$  the value  $\max_{z^* \in Q_0^{\hat{y}}} F(z^*)_{\hat{y}}$  obtains its minimal value  $\frac{1}{L}$  w.r.t.  $z_0$ . In a nutshell, under the restriction of unchangeable non-ME values when generating adversarial examples, normal examples of  $S_{\hat{y}}$  compel adversaries to lower down confidence  $F(z^*)_{\hat{y}}$  the most to  $\frac{1}{L}$  when moving normal examples across the decision boundary. This means that adversarial examples are hardest to craft on the normal examples of  $S_{\hat{y}}$  under the restriction.

According to Theorem 1, if the learned representation transformation:  $x \rightarrow z$  in a DNN classifier can map the normal examples to the neighborhood of  $S_{\hat{y}}$ , then using the new metric non-ME will improve the robustness in the final-layer hidden space and further results in an improvement in the input space. To illustrate this idea, the left panel in Fig. 1 presents an example in the final-layer hidden space, where  $z \in \mathbb{R}^2$  and  $L = 3$ . In this case, all the points that locate on the set  $S_{\hat{y}}$  (black dashed lines in Fig. 1) have highest values of non-ME =  $\log 2$ . For implementation feasibility, we relax the restriction  $z^* \in Q_0^{\hat{y}}$ , and assume that the classifier  $F$  makes all the normal examples have non-ME values higher than a threshold  $t$ , which indicates that the normal examples are all mapped to the neighborhood of  $S_{\hat{y}}$  by the representation transformation. Therefore, given any unidentified input (i.e., adversarial example), if its non-ME value is less than  $t$  the classifier will immediately know that this input is not normal and filters it out.

As depicted in Fig. 1,  $z_0$  is the original normal input, from which an adversary tries to generate adversarial examples.

$z_0$  locates in the neighborhood of  $S_{\hat{y}}$ , where the neighborhood boundary consists of the isolines of non-ME =  $t$  shown by the blue dot-dashed lines. When there is no detection metric, the nearest successful adversarial example is  $z_1$  locating on the nearest decision boundary w.r.t.  $z_0$ . In contrast, when non-ME is used as the detection metric,  $z_1$  will be easily filtered out by the classifier because non-ME( $z_1$ ) is less than  $t$ , and the nearest successful adversarial example becomes  $z_2$  in this case, which locates on the nearest junction manifold of the neighborhood boundary and the decision boundary. Note that the central point  $C$  of the decision boundary in Fig. 1 is actually the singleton set  $S_{\hat{y}} \cap \overline{dd_{\hat{y}}}$  in this case, on which has the lowest confidence  $\frac{1}{L} = \frac{1}{3}$  as indicated by Theorem 1. It is easy to find that the minimal perturbation  $\|z_0 - z_2\|$  is larger than  $\|z_0 - z_1\|$ , almost everywhere. Besides, the confidence for class  $\hat{y}$  at  $z_2$  is lower than it at  $z_1$ , which means that due to the existence of the detector, adversaries have to move the original example further and lower its confidence more, to successfully generate adversarial examples that can fool the detector.

### 3.3. The reverse cross-entropy training procedure

Based on the above analysis, we now design a new training objective to improve the robustness of DNN classifiers. The key is to enforce a DNN classifier to map all the normal instances to the neighborhood of the low-dimensional manifolds  $S_{\hat{y}}$  in the final-layer hidden space. According to Lemma 1, this can be achieved by making the non-maximal elements of  $F(x)$  be as equal as possible, and thus has a high non-ME value for every normal input. Specifically, for a training data  $(x, y)$ , we let  $R_y$  denote its reverse label vector whose  $y$ -th element is zero and other elements equal to  $\frac{1}{L-1}$ . One obvious way to achieve the above goal is to apply the model regularization method termed label smoothing (Szegedy et al., 2016), which can be done by introducing a cross-entropy term between  $R_y$  and  $F(x)$  in the cross-entropy objective:

$$\mathcal{L}_{CE}^{\lambda}(x, y) = \mathcal{L}_{CE}(x, y) - \lambda R_y \cdot \log F(x), \quad (2)$$

where  $\lambda$  is a trade-off parameter. However, it is easy to show that minimizing  $\mathcal{L}_{CE}^{\lambda}$  equals to minimizing the cross-entropy between  $F(x)$  and the  $N$ -dimensional probability vector  $P^{\lambda}$ :

$$P_i^{\lambda} = \begin{cases} \frac{1}{\lambda+1} & i = y \\ \frac{\lambda}{(L-1)(\lambda+1)} & i \neq y \end{cases} \quad (3)$$

Note that  $1_y = P^0$  and  $R_y = P^{\infty}$ . Let  $\theta_{\lambda}^* = \arg \min_{\theta} \mathcal{L}_{CE}^{\lambda}$ , then the prediction  $F(x, \theta_{\lambda}^*)$  will tend to equal to  $P^{\lambda}$ , rather than the ground-truth  $1_y$  when  $\lambda > 0$ . This makes the estimate of  $\theta$  by minimizing  $\mathcal{L}_{CE}^{\lambda}$  be biased. In order to have an unbiased estimator of  $\theta$ , which meets the requirements simultaneously that make the output vector

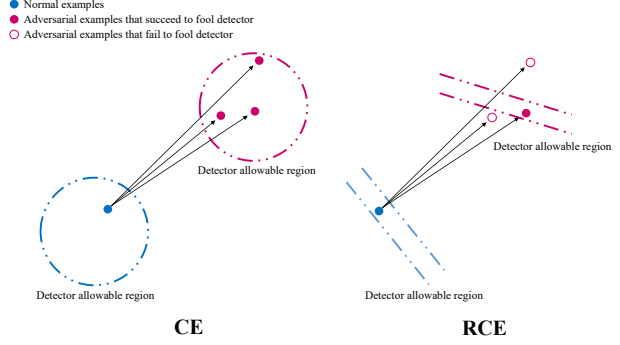


Figure 2. Attacks on networks trained by the RCE procedure require larger and much more elaborate noise. The blue regions are of the original classes for normal examples, and the red regions are of the target classes for adversarial examples.

$F(x)$  tend to  $1_y$  and encourage uniformity among probabilities on untrue classes, we define another objective function based on what we call *reverse cross-entropy (RCE)* as

$$\mathcal{L}_{CE}^R(x, y) = -R_y \cdot \log F(x). \quad (4)$$

Minimizing the RCE is equivalent to minimizing  $\mathcal{L}_{CE}^{\infty}$ . Note that by directly minimizing  $\mathcal{L}_{CE}^R$ , i.e.,  $\theta_R^* = \arg \min_{\theta} \mathcal{L}_{CE}^R$ , one will get a reverse classifier  $F(X, \theta_R^*)$ , which means that given an input  $x$ , the reverse classifier  $F(X, \theta_R^*)$  will not only tend to conceal the index of true class by assigning the lowest probability to it but also tend to output a uniform distribution on other classes.

It is easy to know the class that  $F(X, \theta_R^*)$  wants to conceal the most (i.e., assigns the lowest probability) is actually the true label. This simple insight leads to our RCE training procedure which consists of two parts, as outlined below:

**Reverse training:** Given the training set  $\mathcal{D}$ , we train the DNN  $F(X, \theta)$  to be a reverse classifier by minimizing the average RCE loss:  $\theta_R^* = \arg \min_{\theta} \frac{1}{N} \sum_{d=1}^N \mathcal{L}_{CE}^R(x_d, y_d)$ .

**Reverse logits:** We negate the final logits fed to the softmax layer as  $F_R(X, \theta_R^*) = \mathbb{S}(-Z_{pre}(X, \theta_R^*))$  to get the outputs.

Then we will obtain the network  $F_R(X, \theta_R^*)$  that returns an ordinary distribution on classes, and  $F_R(X, \theta_R^*)$  is referred as the network trained via the RCE training procedure.

**Theorem 2.** (Proof in Appendix) Let  $x$  be a given input in the training dataset,  $y$  be the ground-truth label,  $R_y$  be the reverse label vector of  $y$ ,  $L$  be the number of different classes and  $\theta_R^*$  is obtained from the reverse training. Under the  $L_{\infty}$ -norm, if there is a training error  $\alpha \ll \frac{1}{L}$  that  $\|\mathbb{S}(-Z_{pre}(x, \theta_R^*)) - R_y\|_{\infty} \leq \alpha$ . Then we have bounds

$$\|\mathbb{S}(-Z_{pre}(x, \theta_R^*)) - 1_y\|_{\infty} \leq \alpha(L-1)^2$$

and  $\forall j, k \neq y$

$$|\mathbb{S}(-Z_{pre}(x, \theta_R^*))_j - \mathbb{S}(-Z_{pre}(x, \theta_R^*))_k| \leq 2\alpha^2(L-1)^2.$$

Theorem 2 demonstrates two important properties of the RCE training procedure. First, it is consistent and unbiased in the sense that when the training error  $\alpha \rightarrow 0$ , the output  $F_R(x, \theta_R^*)$  converges to the one-hot label vector  $1_{\hat{y}}$ . Second, the upper bounds of the difference between any two non-maximal elements in outputs decrease much faster in the RCE training than in the CE training w.r.t  $\alpha$ , where the upper bounds decrease as  $\mathcal{O}(\alpha^2)$  for RCE while  $\mathcal{O}(\alpha)$  for CE and label smoothing. These two properties make the RCE training procedure meet our requirements as described above. From now on we do not distinguish between the RCE and the RCE training procedure without ambiguity.

### 3.4. The thresholding test strategy

Given a classifier  $F(X)$  trained via the CE or RCE training procedure, we present a thresholding test strategy as the detector for robust prediction. Presetting a metric and a threshold  $T$ , the detector classifies the input as normal and decides to return the predicted label if the value of metric is larger than  $T$ , or classifies the one as adversarial and returns NOT SURE otherwise. We introduce three candidate metrics as below, and separately test them in Section 4.

**Confidence:** Given an input  $x$ , the corresponding confidence score is calculated as  $\text{Confidence}(x) = F(x)_{\hat{y}}$ .

**non-ME:** According to Eq. (1), the non-ME value is calculated as  $\text{non-ME}(x) = -\sum_{i \neq \hat{y}} \hat{F}(x)_i \log(\hat{F}(x)_i)$ .

**Kernel density:** Since the relatively better robustness and versatility of kernel density estimate method (Feinman et al., 2017; Carlini & Wagner, 2017b), we also choose kernel density as a candidate metric. The kernel density is calculated in the final-layer hidden space, and given the predicted label  $\hat{y}$  and the corresponding training points set  $X_{\hat{y}}$  with label  $\hat{y}$ , the kernel density on the input  $x$  is

$$KD(x) = \frac{1}{|X_{\hat{y}}|} \sum_{x_i \in X_{\hat{y}}} k(z_i, z),$$

where  $z_i$  and  $z$  are the corresponding final-layer hidden vectors.  $k(\cdot, \cdot)$  is the kernel function, which is often chosen as a Gaussian kernel with bandwidth  $\sigma$  as

$$k(z_i, z) = \exp(-\|z_i - z\|^2 / \sigma^2),$$

and the bandwidth  $\sigma$  is treated as a hyperparameter.

## 4. Experiments

In this section, we present both quantitative and qualitative results to demonstrate the effectiveness of the proposed method on improving the robustness of DNN classifiers against various attacking methods.

### 4.1. Setup

We use the two widely studied datasets—MNIST (LeCun et al., 1998) and CIFAR-10 (Krizhevsky & Hinton, 2009). MNIST is a collection of 70k images of handwritten digits in classes 0 to 9. It has a training set of 60k examples and a test set of 10k examples. CIFAR-10 consists of 60k color images in 10 classes with 6k images per class. There are 50k training images and 10k test images. Images in both sets are normalized to be in the interval  $[-0.5, 0.5]$  before fed to classifiers. The normal examples in our experiments refer to all the ones in the training and test sets.

Table 1. Classification error rates (%) on test sets.

Method	MNIST	CIFAR-10
DropConnect (Wan et al., 2013)	0.57	9.32
Maxout (Goodfellow et al., 2013)	0.45	9.38
NiN (Lin et al., 2014)	0.47	8.81
FitNet (Romero et al., 2015)	0.51	8.39
DSN (Lee et al., 2015)	0.39	7.97
R-CNN (Liang & Hu, 2015)	0.31	7.09
Resnet-32 + CE	0.38	7.13
Resnet-32 + RCE	<b>0.29</b>	<b>7.02</b>
Resnet-56 + CE	0.36	<b>6.49</b>
Resnet-56 + RCE	<b>0.32</b>	6.60

### 4.2. Classification on normal examples

We implement Resnet-32 and Resnet-56 (He et al., 2016a) on both datasets. For each network, we use both the CE and RCE as the training objectives, trained by the same settings as He et al. (2016b). The training steps for both objectives are set to be 20k on MNIST and 90k on CIFAR-10. Table 1 provides the classification error rates on test sets, where the thresholding test strategy is disabled and all the points receive their predicted labels. The results show that the classification performance of the networks trained by the RCE is as good as and sometimes even better than those trained by the traditional CE procedure. Note that we apply the same training hyperparameters like learning rates and decay factors for both the CE and RCE procedures, which suggests that the RCE is easy to optimize and does not require much extra effort on tuning hyperparameters.

In order to verify that the RCE training procedure tends to map all the normal inputs to the neighborhood of  $S_{\hat{y}}$  in the final-layer hidden space, we apply the t-SNE technique (Maaten & Hinton, 2008) to visualize the distribution of the final hidden vector  $z$  on the training set. The right two panels in Fig. 1 give the 2-D visualization results. For clarity, we show the results on 1,000 test examples of CIFAR-10. As seen in the results, the networks trained by the RCE can successfully map the test examples to the neighborhood of low-dimensional manifolds in the final-layer hidden space.

Hereafter for notational simplicity, we will directly indicate the training procedure used after the model name of a trained

Table 2. AUC-scores ( $10^{-2}$ ) and average distortions of adversarial examples on MNIST and CIFAR-10. Values are calculated on the examples which are correctly classified as normal examples and then misclassified as adversarial counterparts. Bandwidths used when calculating K-density are  $\sigma_{CE}^2 = 1/0.26$  and  $\sigma_{RCE}^2 = 0.1/0.26$ . **Boldface** indicates the better combination w.r.t the objective, and asterisk \* indicates the best combination under certain attack.

Attack	Objective	Distortion	MNIST			Distortion	CIFAR-10		
			Confidence	AUC-scores ( $10^{-2}$ ) non-ME	K-density		Confidence	AUC-scores ( $10^{-2}$ ) non-ME	K-density
FGSM	CE	26.92	79.7	66.8	98.8	29.80	71.5	66.9	<b>99.7*</b>
	RCE	26.63	<b>98.8</b>	<b>98.6</b>	<b>99.4*</b>	29.81	<b>92.6</b>	<b>91.4</b>	98.0
BIM	CE	6.80	88.9	70.5	90.0	6.29	0.0	64.6	<b>100.0*</b>
	RCE	7.15	<b>91.7</b>	<b>90.6</b>	<b>91.8*</b>	5.46	<b>0.7</b>	<b>70.2</b>	<b>100.0*</b>
ILCM	CE	6.57	98.4	50.4	96.2	2.51	16.4	37.1	84.2
	RCE	6.60	<b>100.0*</b>	<b>97.0</b>	<b>98.6</b>	2.06	<b>64.1</b>	<b>77.8</b>	<b>93.9*</b>
JSMA	CE	12.1	98.6	60.1	97.7	1.53	99.2	27.3	85.8
	RCE	12.87	<b>100.0*</b>	<b>99.4</b>	<b>99.0</b>	1.40	<b>99.5*</b>	<b>91.9</b>	<b>95.4</b>
C&W	CE	8.63	98.6	64.1	99.4	0.65	99.5	50.2	95.3
	RCE	11.04	<b>100.0*</b>	<b>99.5</b>	<b>99.8</b>	0.77	<b>99.6*</b>	<b>94.7</b>	<b>98.2</b>
C&W-hc	CE	13.70	0.0	40.0	91.1	0.93	0.0	28.8	75.4
	RCE	23.20	<b>0.1</b>	<b>93.4</b>	<b>99.6*</b>	1.81	<b>0.2</b>	<b>53.6</b>	<b>91.8*</b>
Average	CE	12.45	77.4	58.7	95.5	6.95	47.8	45.8	90.1
	RCE	14.57	<b>81.8</b>	<b>96.4</b>	<b>98.0*</b>	6.89	<b>59.5</b>	<b>80.0</b>	<b>96.2*</b>

network, e.g., Resnet-32 (CE). Similar, we indicate the training procedure and omit the model name of the target network after an attacking method, e.g., FGSM (CE).

### 4.3. Performance under the oblivious attack

We test the performance of the trained Resnet-32 networks on MNIST and CIFAR-10 under the oblivious attack, where we investigate the attacking methods described in Section 2.3. We first disable the thresholding test strategy and make classifiers return all predictions to study the networks ability of correctly classifying adversarial examples.

We use four gradient-based attacking methods, i.e., FGSM, BIM, ILCM and JSMA, and then we calculate the classification accuracy of networks on crafted adversarial examples w.r.t. the perturbation  $\epsilon$ . We demonstrate the results in Fig. 3. We can find that Resnet-32 (RCE) has higher accuracy than Resnet-32 (CE) under all the four attacks on both datasets. This happens because that when applying gradient-based methods to attack the networks trained by the RCE, the gradients used by the attacking methods are less accurate

as the first-order approximations, which leads to less accurate attacks. However, the adversarial examples crafted by optimization-based methods like C&W can still make Resnet-32 (RCE) misclassify with 100% success rate, since optimization-based methods iterate thousands of times and rely much less on the accuracy of gradients. Note that the attacks on CIFAR-10 are much more efficient than those on MNIST in the sense of requiring smaller perturbations to achieve same attacking success rates, but when adversaries impose large enough perturbations, attacks can still have high success rates on both datasets. That is why the thresholding test strategy is necessary to detect and filter out adversarial examples.

We activate the thresholding test strategy and separately test the performance of three candidate metrics, i.e., *Confidence*, *non-ME* and *Kernel density* (abbr. to *K-density*). We construct simple binary classifiers to decide whether an example is adversarial or not by thresholding with different metrics, and then calculate the AUC-scores of ROC curves on these binary classifiers. Table 2 shows the AUC-scores calculated under different combinations of training procedures and thresholding metrics on both datasets. We also calculate the average distortions introduced in Szegedy et al. (2014) as  $(\sum_{i=1}^d (x_i^* - x_i)^2 / d)^{1/2}$ , where  $x^*$  represents the actual generated adversarial example and each pixel feature is set to be in the interval  $[0, 255]$ . Moreover, in order to make our investigation more convincing, we introduce the high-confidence version of the C&W attack (abbr. to C&W-hc) that sets the parameter  $\kappa$  in the C&W attack to be 10 in our experiments. The C&W-hc attack can generate adversarial examples with the confidence higher than 0.99, and previous work has shown that the adversarial examples

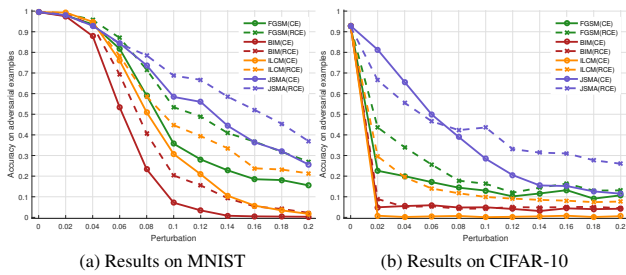


Figure 3. Classification accuracy on adversarial examples.

crafted by C&W-hc are stronger and more difficult to detect than those crafted by C&W (Carlini & Wagner, 2017a;b).

According to the results in Table 2, we find that our method with K-density as the thresholding metric performs better in almost all cases. Besides, non-ME itself is also a pretty reliable metric, although is not as good as K-density since K-density can convey more information than non-ME. Remember that the C&W attack and its variants (e.g., C&W-hc) include modified binary search mechanism to insure finding successful adversarial examples with minimal distortions, our results suggest that the two attacks need much larger minimal distortions to successfully attack on the networks trained by the RCE than on those trained by the CE. Similar phenomenon is also observed under the white-box attack. Another noteworthy phenomenon shown in Table 2 is that the classifiers trained by the RCE return more reliable confidence, which verifies the conclusion in Theorem 1.

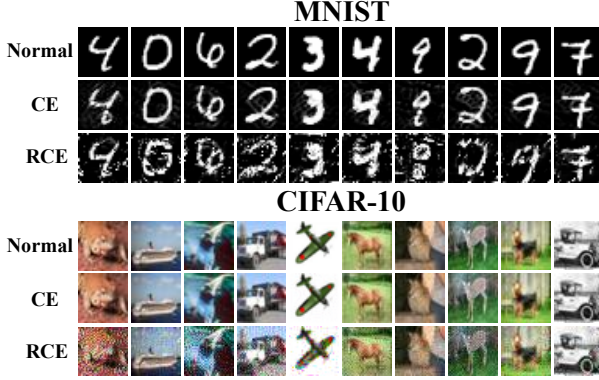


Figure 4. Some normal and adversarial examples from MNIST and CIFAR-10. Adversarial examples are generated by C&W-wb with minimal distortions. The normal test images are termed as *Normal*, and adversarial examples generated on Resnet-32 (CE) and Resnet-32 (RCE) are separately termed as *CE* / *RCE*.

#### 4.4. Performance under the white-box attack

We test our method under the white-box attack, which is the most difficult threat model and no efficient defense exists yet. Due to the prominent performance under the oblivious attack, we select K-density as our thresholding metric. We apply the white-box version of the C&W attack introduced in Carlini & Wagner (2017b), which is constructed specifically to fool the K-density detectors. We refer to this attack as C&W-wb. Compared to the C&W attack, C&W-wb introduces a new loss term  $f_2(x^*)$  that penalizes the adversarial example  $x^*$  being detected by the K-density detectors. The loss  $f_2(x^*) = \max(-\log(KD(x^*)) - \eta, 0)$ , where  $\eta$  is set to be the median of  $-\log(KD(\cdot))$  on the training set.

In practice, we adopt the two-phase implementation procedure of C&W-wb (Carlini & Wagner, 2017b). Table 3 shows the average distortions and the ratios of  $f_2(x^*) > 0$

on the adversarial examples crafted by C&W-wb, where a higher ratio indicates that the detector is more robust and harder to be fooled. We find that nearly all the adversarial examples generated on Resnet-32 (CE) have  $f_2(x^*) \leq 0$ , which means that the values of K-density on them are greater than half of the values on the training data. This result is consistent with previous work (Carlini & Wagner, 2017b).

Table 3. The ratios (%) of  $f_2(x^*) > 0$  and average distortions of the adversarial examples generated by C&W-wb on MNIST and CIFAR-10. The model is Resnet-32 and the metric is K-density.

Objective	MNIST		CIFAR-10	
	Ratio	Distortion	Ratio	Distortion
CE	1	17.12	0	1.26
RCE	77	<b>31.59</b>	<b>12</b>	<b>3.89</b>

However, note that applying C&W-wb on our method has a much higher ratio and results in a much larger minimal distortion. To provide intuitive results, we show some adversarial examples crafted by C&W-wb with the corresponding normal ones in Fig. 4. We find that the adversarial examples crafted on Resnet-32 (CE) are indistinguishable from the normal examples by human eyes. By contrast, those crafted on Resnet-32 (RCE) have macroscopic noises, which are not strictly adversarial examples since they are visually distinguishable from normal examples. The reason why the most aggressive attack C&W-wb becomes inefficient facing our method is illustrated intuitively in Fig. 2. The RCE training procedure in our method conceals normal examples on low-dimensional manifolds in the final-layer hidden space, thus the adversaries who intend to fool our detector have to generate much more elaborate adversarial examples with larger minimal distortions.

Other attacking methods such as the iterative-based ones cannot successfully fool any of the K-density detectors even if there are additional specific losses in their objective functions, since fooling detectors requires much more precise generation than fooling classifiers, which can only be efficiently done by optimization-based attacks.

#### 4.5. Performance under the black-box attack

To completely verify the effectiveness of the proposed method, we investigate the robustness under the black-box attack. The success of the black-box attack is based on the transferability of adversarial examples among different models (Goodfellow et al., 2015).

Table 4. AUC-scores ( $10^{-2}$ ) on CIFAR-10. Resnet-32 is the substitute model and Resnet-56 is the target model.

	Resnet-32 (CE)	Resnet-32 (RCE)
Resnet-56 (CE)	75.0	90.8
Resnet-56 (RCE)	89.1	84.9

We set the trained Resnet-56 networks as the target models,

which adversaries intend to attack but do not have access to their parameters. Thus we set the trained Resnet-32 networks to be the substitute models that adversaries actually attack on and then feed the crafted adversarial examples into the target models. Since adversaries know the existence of the K-density detectors, we apply the C&W-wb attack. We find that the adversarial examples crafted by the C&W-wb attack have poor transferability, where less than 50% of them can make the target model misclassify on MNIST and less than 15% on CIFAR-10. Table 4 shows the AUC-scores in four different cases of the black-box attack on CIFAR-10, and the AUC-scores in the same cases on MNIST are all higher than 95%. Note that in our experiment the target models and the substitute models have very similar structures, and the C&W-wb attack becomes inefficient even under this quite ‘white’ black-box attack.

## 5. Conclusion and future work

In this paper we present a novel method to improve the robustness under different threat models by reliably detecting and filtering out adversarial examples, which performs well on both the MNIST and CIFAR-10 datasets. Our method can be implemented using standard algorithms with little extra training cost. Because of the simplicity, our method is also easy to extend with other defense strategies such as adversarial training (Szegedy et al., 2014). Our main future work is to extend our method to large-scale dataset like ImageNet (Deng et al., 2009), where training via the RCE procedure requires better tuning on hyperparameters.

## References

Bhagoji, Arjun Nitin, Cullina, Daniel, and Mittal, Prateek. Dimensionality reduction as a defense against evasion attacks on machine learning classifiers. *arXiv preprint arXiv:1704.02654*, 2017.

Carlini, Nicholas and Wagner, David. Towards evaluating the robustness of neural networks. *IEEE Symposium on Security and Privacy*, 2017a.

Carlini, Nicholas and Wagner, David. Adversarial examples are not easily detected: Bypassing ten detection methods. *ACM Workshop on Artificial Intelligence and Security*, 2017b.

Deng, Jia, Dong, Wei, Socher, Richard, Li, Li-Jia, Li, Kai, and Fei-Fei, Li. Imagenet: A large-scale hierarchical image database. In *Proceedings of the IEEE Conference on Computer Vision and Pattern Recognition (CVPR)*, pp. 248–255. IEEE, 2009.

Feinman, Reuben, Curtin, Ryan R, Shintre, Saurabh, and Gardner, Andrew B. Detecting adversarial samples from artifacts. *arXiv preprint arXiv:1703.00410*, 2017.

Gong, Zhitao, Wang, Wenlu, and Ku, Wei-Shinn. Adversarial and clean data are not twins. *arXiv preprint arXiv:1704.04960*, 2017.

Goodfellow, Ian, Bengio, Yoshua, and Courville, Aaron. *Deep Learning*. MIT Press, 2016. <http://www.deeplearningbook.org>.

Goodfellow, Ian J, Warde-Farley, David, Mirza, Mehdi, Courville, Aaron, and Bengio, Yoshua. Maxout networks. *International Conference on Machine Learning (ICML)*, 2013.

Goodfellow, Ian J, Shlens, Jonathon, and Szegedy, Christian. Explaining and harnessing adversarial examples. *The International Conference on Learning Representations (ICLR)*, 2015.

Grosse, Kathrin, Manoharan, Praveen, Papernot, Nicolas, Backes, Michael, and McDaniel, Patrick. On the (statistical) detection of adversarial examples. *arXiv preprint arXiv:1702.06280*, 2017.

Gu, Shixiang and Rigazio, Luca. Towards deep neural network architectures robust to adversarial examples. *Conference on Neural Information Processing Systems (NIPS) Workshops*, 2014.

He, Kaiming, Zhang, Xiangyu, Ren, Shaoqing, and Sun, Jian. Deep residual learning for image recognition. In *Proceedings of the IEEE Conference on Computer Vision and Pattern Recognition (CVPR)*, pp. 770–778, 2016a.

He, Kaiming, Zhang, Xiangyu, Ren, Shaoqing, and Sun, Jian. Identity mappings in deep residual networks. In *European Conference on Computer Vision (ECCV)*, pp. 630–645. Springer, 2016b.

Hornik, Kurt, Stinchcombe, Maxwell, and White, Halbert. Multilayer feedforward networks are universal approximators. *Neural networks*, 2(5):359–366, 1989.

Kingma, Diederik and Ba, Jimmy. Adam: A method for stochastic optimization. *The International Conference on Learning Representations (ICLR)*, 2015.

Krizhevsky, Alex and Hinton, Geoffrey. Learning multiple layers of features from tiny images. Technical report, 2009.

Kurakin, Alexey, Goodfellow, Ian, and Bengio, Samy. Adversarial examples in the physical world. *The International Conference on Learning Representations (ICLR) Workshops*, 2017a.

Kurakin, Alexey, Goodfellow, Ian, and Bengio, Samy. Adversarial machine learning at scale. *The International Conference on Learning Representations (ICLR)*, 2017b.

LeCun, Yann, Bottou, Léon, Bengio, Yoshua, and Haffner, Patrick. Gradient-based learning applied to document recognition. *Proceedings of the IEEE*, 86(11):2278–2324, 1998.

Lee, Chen-Yu, Xie, Saining, Gallagher, Patrick, Zhang, Zhengyou, and Tu, Zhuowen. Deeply-supervised nets. In *Artificial Intelligence and Statistics*, pp. 562–570, 2015.

Li, Xin and Li, Fuxin. Adversarial examples detection in deep networks with convolutional filter statistics. *arXiv preprint arXiv:1612.07767*, 2016.

Li, Yingzhen and Gal, Yarin. Dropout inference in bayesian neural networks with alpha-divergences. *International Conference on Machine Learning (ICML)*, 2017.

Liang, Ming and Hu, Xiaolin. Recurrent convolutional neural network for object recognition. In *Proceedings of the IEEE Conference on Computer Vision and Pattern Recognition (CVPR)*, pp. 3367–3375. IEEE, 2015.

Lin, Min, Chen, Qiang, and Yan, Shuicheng. Network in network. *The International Conference on Learning Representations (ICLR)*, 2014.

Liu, Yanpei, Chen, Xinyun, Liu, Chang, and Song, Dawn. Delving into transferable adversarial examples and black-box attacks. *The International Conference on Learning Representations (ICLR)*, 2017.

Maaten, Laurens van der and Hinton, Geoffrey. Visualizing data using t-sne. *Journal of Machine Learning Research (JMLR)*, 9(Nov):2579–2605, 2008.

Metzen, Jan Hendrik, Genewein, Tim, Fischer, Volker, and Bischoff, Bastian. On detecting adversarial perturbations. *The International Conference on Learning Representations (ICLR)*, 2017.

Nguyen, Anh, Yosinski, Jason, and Clune, Jeff. Deep neural networks are easily fooled: High confidence predictions for unrecognizable images. In *The IEEE Conference on Computer Vision and Pattern Recognition (CVPR)*, pp. 427–436, 2015.

Papernot, Nicolas, McDaniel, Patrick, Goodfellow, Ian, Jha, Somesh, Celik, Z Berkay, and Swami, Ananthram. Practical black-box attacks against deep learning systems using adversarial examples. *arXiv preprint arXiv:1602.02697*, 2016a.

Papernot, Nicolas, McDaniel, Patrick, Jha, Somesh, Fredrikson, Matt, Celik, Z Berkay, and Swami, Ananthram. The limitations of deep learning in adversarial settings. In *Security and Privacy (EuroS&P), 2016 IEEE European Symposium on*, pp. 372–387. IEEE, 2016b.

Papernot, Nicolas, McDaniel, Patrick, Wu, Xi, Jha, Somesh, and Swami, Ananthram. Distillation as a defense to adversarial perturbations against deep neural networks. In *Security and Privacy (SP), 2016 IEEE Symposium on*, pp. 582–597. IEEE, 2016c.

Romero, Adriana, Ballas, Nicolas, Kahou, Samira Ebrahimi, Chassang, Antoine, Gatta, Carlo, and Bengio, Yoshua. Fitnets: Hints for thin deep nets. *The International Conference on Learning Representations (ICLR)*, 2015.

Rozsa, Andras, Rudd, Ethan M, and Boult, Terrance E. Adversarial diversity and hard positive generation. In *Proceedings of the IEEE Conference on Computer Vision and Pattern Recognition (CVPR) Workshops*, pp. 25–32, 2016.

Rumelhart, David E, Hinton, Geoffrey E, and Williams, Ronald J. Learning representations by back-propagating errors. *Cognitive modeling*, 5(3):1, 1988.

Szegedy, Christian, Zaremba, Wojciech, Sutskever, Ilya, Bruna, Joan, Erhan, Dumitru, Goodfellow, Ian, and Fergus, Rob. Intriguing properties of neural networks. *The International Conference on Learning Representations (ICLR)*, 2014.

Szegedy, Christian, Vanhoucke, Vincent, Ioffe, Sergey, Shlens, Jon, and Wojna, Zbigniew. Rethinking the inception architecture for computer vision. In *Proceedings of the IEEE Conference on Computer Vision and Pattern Recognition (CVPR)*, pp. 2818–2826, 2016.

Wan, Li, Zeiler, Matthew, Zhang, Sixin, Le Cun, Yann, and Fergus, Rob. Regularization of neural networks using dropconnect. In *International Conference on Machine Learning (ICML)*, pp. 1058–1066, 2013.

Zheng, Stephan, Song, Yang, Leung, Thomas, and Goodfellow, Ian. Improving the robustness of deep neural networks via stability training. In *The IEEE Conference on Computer Vision and Pattern Recognition (CVPR)*, June 2016.

## A. Proof

**Lemma 1.** *In the decision region  $dd_{\hat{y}}$  of class  $\hat{y}$ ,  $\forall i, j \neq \hat{y}, \widetilde{db}_{ij} \in DB_{ij}$ , the value of non-ME on any low-dimensional manifold  $\bigcap_{i,j \neq \hat{y}} \widetilde{db}_{ij}$  is constant. In particular, non-ME obtains its global maximal value  $\log(L-1)$  on and only on  $S_{\hat{y}}$ .*

*Proof.*  $\forall i, j \neq \hat{y}$ , we take a hyperplane  $\widetilde{db}_{ij} \in DB_{ij}$ . Then according to the definition of the set  $DB_{ij}$ , it is easily shown that  $\forall z \in \widetilde{db}_{ij}$ ,  $Z_{pre,i} - Z_{pre,j} = \text{constant}$ , and we denote this corresponding constant as  $C_{ij}$ . Thus given any  $k \neq \hat{y}$ , we derive that  $\forall z \in \bigcap_{i,j \neq \hat{y}} \widetilde{db}_{ij}$

$$\begin{aligned} \hat{F}(z)_k &= \frac{F(z)_k}{\sum_{j \neq \hat{y}} F(z)_j} \\ &= \frac{\exp(Z_{pre,k})}{\sum_{j \neq \hat{y}} \exp(Z_{pre,j})} \\ &= \frac{1}{\sum_{j \neq \hat{y}} \exp(Z_{pre,j} - Z_{pre,k})} \\ &= \frac{1}{\sum_{j \neq \hat{y}} \exp(C_{jk})} \\ &= \text{constant}, \end{aligned}$$

and according to the definition of the non-ME value  $\text{non-ME}(z) = -\sum_{i \neq \hat{y}} \hat{F}(z)_i \log(\hat{F}(z)_i)$ , we can conclude that  $\text{non-ME}(z) = \text{constant}, \forall z \in \bigcap_{i,j \neq \hat{y}} \widetilde{db}_{ij}$ .

In particular, according to the property of entropy in information theory, we know that  $\text{non-ME} \leq \log(L-1)$ , and non-ME achieve its maximal value if and only if  $\forall k \neq \hat{y}, \hat{F}_k = \frac{1}{L-1}$ . In this case, there is  $\forall i, j \neq \hat{y}, Z_{pre,i} = Z_{pre,j}$ , which is easy to show that the conditions hold on  $S_{\hat{y}}$ . Conversely,  $\forall z \notin S_{\hat{y}}$ , there must  $\exists i, j \neq \hat{y}$ , such that  $Z_{pre,i} \neq Z_{pre,j}$  which leads to  $\hat{F}_i \neq \hat{F}_j$ . This violates the condition of non-ME achieving its maximal value. Thus non-ME obtains its global maximal value  $\log(L-1)$  on and only on  $S_{\hat{y}}$ .

□

**Theorem 1.** *In the decision region  $dd_{\hat{y}}$  of class  $\hat{y}$ ,  $\forall i, j \neq \hat{y}, z_0 \in dd_{\hat{y}}$ , there exists a unique  $\widetilde{db}_{ij}^0 \in DB_{ij}$ , such that  $z_0 \in Q_0$ , where  $Q_0 = \bigcap_{i,j \neq \hat{y}} \widetilde{db}_{ij}^0$ . Let  $Q_0^{\hat{y}} = Q_0 \cap \overline{dd_{\hat{y}}}$ , then the solution set of the problem*

$$\arg \min_{z_0} \left( \max_{z^* \in Q_0^{\hat{y}}} F(z^*)_{\hat{y}} \right)$$

is  $S_{\hat{y}}$ . Furthermore  $\forall z_0 \in S_{\hat{y}}$  there is  $Q_0 = S_{\hat{y}}$ , and  $\forall z^* \in S_{\hat{y}} \cap \overline{dd_{\hat{y}}}, F(z^*)_{\hat{y}} = \frac{1}{L}$ .

*Proof.* It is easy to show that given a point and a normal vector, one can uniquely determine a hyperplane. Thus  $\forall i, j \neq \hat{y}, z_0 \in dd_{\hat{y}}$ , there exists unique  $\widetilde{db}_{ij}^0 \in DB_{ij}$ , such that  $z_0 \in \bigcap_{i,j \neq \hat{y}} \widetilde{db}_{ij}^0 = Q_0$ .

According to the proof of Lemma 1, we have  $\forall i, j \neq \hat{y}, z^* \in Q_0^{\hat{y}}$ , there is  $Z_{pre,i} - Z_{pre,j} = C_{ij}$ , and  $\exists k \neq \hat{y}$ , s. t.  $Z_{pre,\hat{y}} = Z_{pre,k}$ . Thus we can derive

$$\begin{aligned} F(z^*)_{\hat{y}} &= \frac{\exp(Z_{pre,\hat{y}})}{\sum_i \exp(Z_{pre,i})} \\ &= \frac{1}{1 + \sum_{i \neq \hat{y}} \exp(Z_{pre,i} - Z_{pre,\hat{y}})} \\ &= \frac{1}{1 + \exp(Z_{pre,k} - Z_{pre,\hat{y}})(1 + \sum_{i \neq \hat{y}, k} \exp(Z_{pre,i} - Z_{pre,k}))} \\ &= \frac{1}{2 + \sum_{i \neq \hat{y}, k} \exp(C_{ik})}. \end{aligned}$$

Let  $M = \{i : C_{ij} \geq 0, \forall j \neq \hat{y}\}$ , there must be  $k \in M$  so  $M$  is not empty, and we have

$$\begin{aligned} \max_{z^* \in Q_0^{\hat{y}}} F(z^*)_{\hat{y}} &= \max_{l \in M} \frac{1}{2 + \sum_{i \neq \hat{y}, l} \exp(C_{il})} \\ &= \frac{1}{2 + \min_{l \in M} \sum_{i \neq \hat{y}, l} \exp(C_{il})} \\ &= \frac{1}{2 + \sum_{i \neq \hat{y}, \tilde{k}} \exp(C_{i\tilde{k}})}, \end{aligned}$$

where  $\tilde{k}$  is any element in  $M$ . This equation holds since  $\forall k_1, k_2 \in M$ , there is  $C_{k_1 k_2} \geq 0, C_{k_2 k_1} \geq 0$  and  $C_{k_1 k_2} = -C_{k_2 k_1}$ , which leads to  $C_{k_1 k_2} = C_{k_2 k_1} = 0$ . Therefore,  $\forall l \in M, \sum_{i \neq \hat{y}, l} \exp(C_{il})$  has the same value.

This equation consequently results in

$$\begin{aligned} \arg \min_{z_0} \left( \max_{z^* \in Q_0^{\hat{y}}} F(z^*)_{\hat{y}} \right) &= \arg \min_{z_0} \frac{1}{2 + \sum_{i \neq \hat{y}, \tilde{k}} \exp(C_{i\tilde{k}})} \\ &= \arg \max_{z_0} \sum_{i \neq \hat{y}, \tilde{k}} \exp(C_{i\tilde{k}}). \end{aligned}$$

From the conclusion in Lemma 1, we know that the value  $\sum_{i \neq \hat{y}, \tilde{k}} \exp(C_{i\tilde{k}})$  obtains its maximum when  $C_{i\tilde{k}} = 0, \forall i \neq \hat{y}, \tilde{k}$ . Thus the solution set of the above problem is  $S_{\hat{y}}$ . Furthermore, we have  $\forall z^* \in S_{\hat{y}} \cap \overline{dd_{\hat{y}}}, F(z^*)_{\hat{y}} = \frac{1}{2+L-2} = \frac{1}{L}$ .

□

**Theorem 2.** Let  $x$  be a given input in the training dataset,  $y$  be the ground-truth label,  $R_y$  be the reverse label vector of  $y$ ,  $L$  be the number of different classes and  $\theta_R^*$  is obtained from the reverse training. Under the  $L_\infty$ -norm, if there is a training error  $\alpha \ll \frac{1}{L}$  that  $\|\mathbb{S}(Z_{pre}(x, \theta_R^*)) - R_y\|_\infty \leq \alpha$ . Then we have bounds

$$\|\mathbb{S}(-Z_{pre}(x, \theta_R^*)) - 1_y\|_\infty \leq \alpha(L-1)^2$$

and  $\forall j, k \neq y$

$$|\mathbb{S}(-Z_{pre}(x, \theta_R^*))_j - \mathbb{S}(-Z_{pre}(x, \theta_R^*))_k| \leq 2\alpha^2(L-1)^2.$$

*Proof.* For simplicity we omit the dependence of the logits  $Z_{pre}$  on the input  $x$  and the parameters  $\theta_R^*$ . Let  $G = (g_1, g_2, \dots, g_L)$  be the exponential logits, where  $g_i = \exp(Z_{pre,i})$ . Then from the condition  $\|\mathbb{S}(Z_{pre}) - R_y\|_\infty \leq \alpha$  we have

$$\begin{cases} \frac{g_y}{\sum_i g_i} \leq \alpha \\ \left| \frac{g_j}{\sum_i g_i} - \frac{1}{L-1} \right| \leq \alpha \quad j \neq y. \end{cases}$$

Let  $C = \sum_i g_i$ , we can further write the condition as

$$\begin{cases} g_y \leq \alpha C \\ \left( \frac{1}{L-1} - \alpha \right) C \leq g_j \leq \left( \frac{1}{L-1} + \alpha \right) C \quad j \neq y. \end{cases}$$

Then we can have bounds ( $L \geq 2$ )

$$\begin{aligned} \mathbb{S}(-Z_{pre})_j &= \frac{\frac{1}{g_j}}{\frac{1}{g_y} + \sum_{i \neq y} \frac{1}{g_i}} \\ &= \frac{\frac{g_y}{g_j}}{1 + \frac{g_y}{g_j} + \sum_{i \neq y, j} \frac{g_y}{g_i}} \\ &\leq \frac{\frac{g_y}{g_j}}{1 + \frac{g_y}{g_j}} \\ &= \frac{1}{1 + \frac{g_j}{g_y}} \\ &\leq \frac{1}{1 + \frac{(\frac{1}{L-1} - \alpha)C}{\alpha C}} \\ &= \alpha(L-1) \\ &\leq \alpha(L-1)^2. \end{aligned}$$

Then we have proven that  $\|\mathbb{S}(-Z_{pre}) - 1_y\|_\infty \leq \alpha(L-1)^2$ . Furthermore, we have  $\forall j, k \neq y$ ,

$$\begin{aligned} |\mathbb{S}(-Z_{pre})_j - \mathbb{S}(-Z_{pre})_k| &= \frac{\left| \frac{1}{g_j} - \frac{1}{g_k} \right|}{\frac{1}{g_y} + \sum_{i \neq y} \frac{1}{g_i}} \\ &\leq \frac{\frac{1}{(\frac{1}{L-1} - \alpha)C} - \frac{1}{(\frac{1}{L-1} + \alpha)C}}{\frac{1}{\alpha C} + \sum_{i \neq y} \frac{1}{(\frac{1}{L-1} + \alpha)C}} \\ &= \frac{\frac{L-1}{1-\alpha(L-1)} - \frac{L-1}{1+\alpha(L-1)}}{\frac{1}{\alpha} + \frac{(L-1)^2}{1+\alpha(L-1)}} \\ &= \frac{2\alpha^2(L-1)^2}{1 + \alpha(L-1)^2(1 - \alpha L)} \\ &\leq 2\alpha^2(L-1)^2. \end{aligned}$$

□

$$\begin{aligned} \mathbb{S}(-Z_{pre})_y &= \frac{\frac{1}{g_y}}{\frac{1}{g_y} + \sum_{i \neq y} \frac{1}{g_i}} \\ &= \frac{1}{1 + \sum_{i \neq y} \frac{g_y}{g_i}} \\ &\geq \frac{1}{1 + \sum_{i \neq y} \frac{\alpha C}{(\frac{1}{L-1} - \alpha)C}} \\ &= \frac{1}{1 + \frac{\alpha(L-1)^2}{1-\alpha(L-1)}} \\ &= 1 - \frac{\alpha(L-1)^2}{1 - \alpha(L-1) + \alpha(L-1)^2} \\ &\geq 1 - \alpha(L-1)^2 \end{aligned}$$

and  $\forall j \neq y$ ,